ELSEVIER

Catalysis Today 79–80 (2003) 371–381

CATALYSIS TODAY

www.elsevier.com/locate/cattod

Deep desulfurization of middle distillates: process adaptation to oil fractions' compositions

Esteban Pedernera, Rainer Reimert, Ngoc Luan Nguyen*, Vincent van Buren

Division of Fuel Technology, Universität Karlsruhe (TH), Engler-Bunte-Ring 1, 76131 Karlsruhe, Germany

Abstract

The influence of oil fractions' compositions on the conversion of sulfurous components was investigated in a trickle-bed reactor in laboratory scale. A commercially available NiMo/γ-Al_2O_3 catalyst was used throughout the investigations. Experimental results including sulfur conversion of different oil fractions and residence time distributions under reacting conditions are presented. The hydrogen consumption is ascribed to the conversion of sulfur and of nitrogen, to the hydrogenation of aromatics and to hydrocracking based on a simulation applying ASPEN Plus®. Various configurations of the desulfurization process are evaluated but no advantage is found by separate treatment of individual oil fractions. In addition, experiments were carried out to determine liquid distribution and wetting efficiency in a catalyst bed by using magnetic resonance imaging (MRI) technique.

Keywords: Magnetic resonance imaging; Desulfurization; Sulfur

1. Introduction

Hydrodesulfurization has been used in refineries for over 50 years to reduce the sulfur content in diesel fuel to match the applicable legal specifications. Environmental consideration is the major driver for the reduction of the maximum allowable sulfur content. In future so called zero sulfur fuels (below 10 ppm S) will be required for the application of new exhaust gas cleaning technologies introduced by automobile manufacturers [1]. As a consequence, refineries need to increase again the conversion in their desulfurization processes. To achieve higher conversion without excessive increase in the consumption of hydrogen and energy, a proper process understanding of dehydrogenation reactions and reactor hydrodynamics is necessary.

From gas phase experiments it is known that the hydrogenation of specific sulfur compounds or groups is heavily affected by the base oil's composition ("matrix"). The matrix effect may lead to differences in reaction temperature necessary for 50% conversion of up to 40 °C. The influence of the oil matrix could well be correlated with the total sulfur content of the base oil [2]. The authors suggest that polyaromatic sulfur compounds, by addition of one hydrogen atom, react to rather stable, strongly chemisorbed intermediates producing an inhibiting effect.

To exploit these findings for the design and the operation of commercial units, modeling of the reactor and the process is necessary. Due to the complexity of the reaction system only modeling of part of reaction is normally considered [3].

* Corresponding author. Tel.: +49-721-608-2575; fax: +49-721-606-172.
E-mail address: ngoc-luan.nguyen@ciw.uni-karlsruhe.de (N.L. Nguyen).

0920-5861/03/$ – see front matter
doi:10.1016/S0920-5861(03)00066-X

Nomenclature

a_p	specific gas–liquid interface (m^{-1})
A	surface area (m^2)
Ar–N	aromatic nitrogen compound
Ar–S	aromatic sulfur compound
Bo	Bodenstein number ($uL/D_{axial\ of\ liquid}$)
c	concentration ($kmol/m^3$)
$(c/c_0)_{Step}$	Squalan concentration to inlet concentration
C_{Crack}	cracking product compound
C_1	hydrocarbons
d	diameter (mm)
D_{axial}	axial effective diffusivity (m^2/s)
F	mass flow rate (kg/h)
h_p	enthalpy change of total mixture with temperature (kJ/kmol K)
ΔH	heat of reaction (kJ/kmol)
k	reaction rate coefficient $\left([kmol/(kg_{cat}\,h)]^{1-\sum n}\right)$
k_l	mass transfer coefficient gas to liquid $\left(kmol^{1-\sum n}\,m^{3\sum n}/kg_{cat}\,h\right)$
K	adsorption coefficient (m^3/kmol)
L	total reactor length (m)
LGO	light gasoil
LHSV	liquid hourly space velocity (h^{-1})
m_{cat}	total catalyst mass (kg)
M	molecular weight (g/mol)
n	reaction order
N	mole flow rate (kmol/h)
p	total or partial pressure (bar)
Q	volumetric flow rate (m^3/s)
r	rate of heterogeneous reaction ($kmol/kg_{cat}\,h$)
Re	Reynolds number
SGO	heavy gasoil
t	residential time (h)
$t_{1/2}$	mean residential time (h)
T	temperature (°C)
u	superficial velocity (mm/s)
X	conversion (%)
y	volume percent (%)
z	axial coordinate along the length of the reactor (m)

Greek letters

β	liquid saturation, dimensionless
β_h	liquid holdup, dimensionless
γ	wetting efficiency, dimensionless
ζ	fractional volume of catalyst in the packed reactor bed, $[V_{cat}/(V_{cat}+V_{inert})]$, dimensionless
η	viscosity ($N\,s/m^2$)
ν	stoichiometric coefficient, dimensionless
ρ	density (kg/m^3)

Subscripts

b	bulk
Di	diaromatic
g	gas
l	liquid
Mono	monoaromatic
N	at normal conditions
Naph	naphthalene
p	particle
Poly	polyaromatic
R	reactor
S	sulfur

Superscript

$*$	at equilibrium

2. Experimental

The properties of the gasoil used in the investigation are shown in Table 1. This straight run gasoil was courteously supplied by MiRO-Refinery in Karlsruhe, Germany.

The bench scale trickle-bed reactor used is of 19 mm diameter and has a length of 500 mm of which 250 mm were filled with catalyst (Criterion 424) and a diluent (SiC), mixed in a ratio of 1:1.25 (v/v). Diluent

Table 1
Properties of feed gasoil

	Arabian Heavy
S (wt.%)	1.674
Total aromatics (wt.%)	33.5
N (wt. ppm)	195
IBP (0.5 vol.%)–FBP (95 vol.%)	180–395
Average boiling point (°C, 50 vol.%)	337
Density (kg/m^3)	861

diameter is 0.17–0.22 mm in range and catalyst diameter is 1.6 mm with 3.5 mm in length. The dilution with small particles of SiC serves for an efficient radial heat transfer and a more uniform distribution of the fluid over the cross-section of the reactor. The catalyst was activated in the sulfide form by dosing for 21 h a mixture of gasoil and dimethyl disulfide with a total content of 2.9 wt.% of S, while the temperature increased by 10 K/h. After 4 days of operation the catalyst reached a nearly steady state with respect to deactivation. Using a metering pump the gasoil was fed together with the gaseous reactant mix consisting of hydrogen and hydrogen sulfide. Isothermal conditions (max. 2 K deviation) were secured with four electrical heaters.

The sulfur contents of the samples (before and after desulfurization) were determined by an energy dispersive X-ray fluorescence spectrometer (Oxford Lab X 300). Before measuring, the samples were purged with nitrogen to strip dissolved H_2S. Sulfur compounds and groups were selectively determined with high resolution gas chromatography equipped with a selective pulsed flame photometric detector (Varian STAR 3400). The hydrocarbons were detected with a FID. Nitrogen compounds were analyzed by gas chromatography (HP 5890 Series II Plus) with NPD detector.

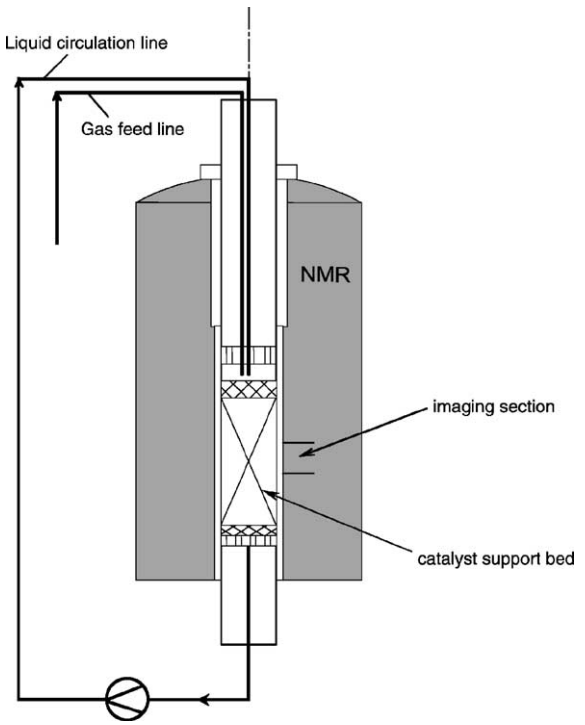

Fig. 1. Schematic diagram of the experimental set-up for MRI measurements.

Total aromatics were determined by elution chromatography (ASTM D-2549). The concentrations of aromatic compounds (mono-, di-, polyaromatics) were determined from the signals of a gas chromatograph mass spectrometer processed by a FORTRAN program (ASTM D-3239-91). Naphthalenes were determined from the non-aromatic part of the elution chromatography by ASTM D-2425-93.

Magnetic resonance imaging (MRI) technique was used to investigate the liquid distribution in the trickle-bed reactor and the wetting efficiency of the catalyst particles [4,5]. Two-dimensional and three-dimensional magnetic resonance images were acquired for flow of air and water within the packed bed at atmospheric conditions. For this experiment the same dimensions of the trickle-bed column as well as of the trilobe formed catalyst support material were used as in the investigations regarding reaction kinetics (Fig. 1).

3. Mathematical model

For the evaluation of the process an extension of the mathematical model presented by Chowdhury et al. [6] is used. The model is fully integrated in Aspen Plus in a User Model Block. The following reactions and respective rate equations were included.

3.1. Sulfur

$$\mathrm{Ar{-}S} + 2\mathrm{H_2} \rightarrow \mathrm{Ar} + \mathrm{H_2S} \quad (1)$$

$$r_{\mathrm{Ar-S}} = -\frac{k_{\mathrm{Ar-S}}(c_{\mathrm{Ar-S}})^{1.4}(c_{\mathrm{H_2}})^{0.5}}{(1 + K_{\mathrm{H_2S}}c_{\mathrm{H_2S}})^2} \quad (2)$$

The reaction systems for sulfur and nitrogen are well studied [11]. Due to analytical limitations and to the large quantity of components in real mixtures some simplifications need to be made to overcome this problem. Reaction orders are estimated from experimental data. Contribution to the hydrogen consumption due to hydrogenation of the aromatic rings from pure

aromatics but also aromatics containing sulfur and nitrogen will be considered via Eqs. (3)–(5). Identification of these two types of aromatic compounds in the mixture is not possible with the applied analytical methods.

3.2. Aromatics

$$\text{Polyaromatic} + H_2 \rightleftarrows \text{Diaromatic} \quad (3)$$

$$\text{Diaromatic} + 2H_2 \rightleftarrows \text{Monoaromatic} \quad (4)$$

$$\text{Monoaromatic} + 3H_2 \rightleftarrows \text{Naphthalene} \quad (5)$$

To calculate the hydrogen consumption due to aromatics' hydrogenation from the analytical results, the molecular weight of each group is needed. The average molecular weight calculated from the results of the simulated distillation of the oil (ASTM D2887) are: $M_{\text{Poly}} = 278\,\text{g/mol}$, $M_{\text{Di}} = 280\,\text{g/mol}$, $M_{\text{Mono}} = 284\,\text{g/mol}$.

As no detailed information could be gathered from the experiments for hydrogenation as well as for dehydrogenation/condensation reactions basic rate expressions were used:

Hydrogenation

$$r_i = -k_i c_i p_{H_2}^{n_i},$$
$$i = \text{ring number (Mono} = 1, \text{Di} = 2, \text{Poly} = 3) \quad (6)$$

Reaction orders are $n_1 = 1$, $n_2 = 0.5$ and $n_3 = 0.5$

Dehydrogenation/condensation

$$r_j = -k_j c_j, \quad j = \text{naphthalene or ring number} \quad (7)$$

3.3. Nitrogen

$$\text{Ar–N} + 2H_2 \rightarrow \text{Ar} + NH_3 \quad (8)$$

$$r_{\text{Ar–N}} = -k_{\text{Ar–N}} (c_{\text{Ar–N}})^{1.1} (c_{H_2})^{0.8} \quad (9)$$

3.4. Hydrocracking

$$C_{C_{16}H_{34}} + 7H_2 \rightarrow C_{\text{crack}} \quad (10)$$

$$r_{\text{crack}} = -k_{\text{crack}} (c_{C_{16}H_{34}})^1 \quad (11)$$

The stoichiometrical equation for hydrocracking is adapted to simulate the experimental hydrogen consumption. The reaction rate is estimated from experimental results taken from the gas phase from the generated cracking compounds C_1–C_8 (added in C_{crack}). Isomerisation is not considered.

Balances are made for H_2 and H_2S in the gas phase and for H_2S and all the other species as per above in the liquid phase assuming stationary conditions in any case:

Gas phase: $0 \le z \le L$

$$u_g \frac{dc_i^g}{dz} + k_i^l a_p (c_i^* - c_i^l) = 0 \quad (12)$$

Liquid phase: $0 \le z \le L$

$$u_l \frac{dc_i^l}{dz} - k_i^l a_p (c_i^* - c_i^l) - \nu_i \rho_b \zeta r = 0 \quad (13)$$

At initial conditions gas and liquid are considered to be in physical equilibrium.

For the mass transfer coefficient k_i empirical expressions are taken from [10]. All physical properties are generated with Aspen Plus (Grayson equation of state and API correlation). More details about the modeling can be found in [6].

For modeling the industrial reactor which operates under nearly adiabatic conditions, a simplified heat balance is done

$$\frac{dT}{dz} = \frac{r_{H_2} \Delta_R H_{\text{HDS}} A_{\text{reactor}} \rho_b \zeta}{N_{\text{total}} h_{\text{p,gas–liquid}}(T)} \quad (14)$$

Under industrial conditions pressure drop and total liquid saturation are calculated with the empirical equations from Wammes et al. [7]. The details of the simulation in Aspen Plus and the user routine with fitted kinetic parameters will be available soon [9].

4. Results and discussion

4.1. Reactor characterization

The reactor flow behavior was analyzed via residence time distribution measurements under reaction conditions. For this purpose a 1.0 wt.% step of Squalan (2,6,10,15,19,23-hexamethyltetracosane, $C_{30}H_{62}$) was added as inert tracer to the gasoil and samples were taken one per minute. To evaluate the response measurements the dispersion model was used.

The results, exemplified for one set of operating conditions in Fig. 2, confirmed that the trickle-bed

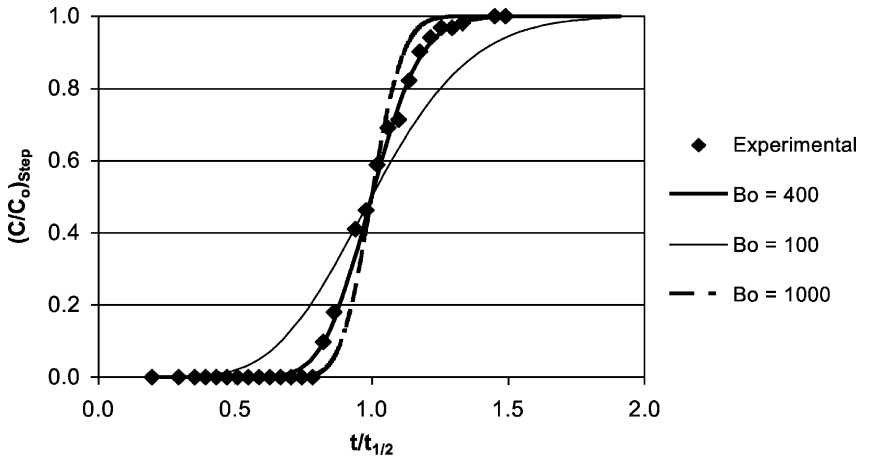

Fig. 2. Calculated (lines) response curves for dispersion model for different *Bo* numbers (Arabian Heavy, $T = 320\,^{\circ}\mathrm{C}$, $p = 40\,\mathrm{bar}$, $\mathrm{LHSV} = 2\,\mathrm{h}^{-1}$, $Q_g/Q_l = 200\,\mathrm{m}^3/\mathrm{m}^3$).

with dilution of catalyst is working at near plug-flow conditions ($Bo = 400$).

To measure the liquid saturation the reactor was run under steady-state reaction conditions. The flow of feed to the reactor was halted and the liquid was totally removed from the reactor by drainage and drying (heated up to 380 °C and purged under normal pressure with nitrogen for 4 h).

The results reported in Table 2 show that the influence of reaction conditions on the liquid holdup might not be neglected. For the presented model the change in liquid saturation β is not included in the balances. Measurements of the dynamic and the static liquid saturation are necessary for a valid extension of the model.

Table 2
Experimental total liquid saturation under reaction conditions

Temperature (°C)	Pressure (bar)	LHSV (h^{-1})	$Q_{gas/oil}$ (m^3/m^3)	β_h
300	40	2	200	0.6
320	40	2	200	0.56
340	40	2	200	0.54
360	40	2	200	0.5
380	40	2	200	0.46
320	20	2	200	0.61
320	60	2	200	0.5
320	40	1	100	0.49
320	40	4	500	0.63
320	40	2	100	0.55
320	40	2	500	0.54

4.2. Results from MRI measurements

In this paper the potential of MRI is presented for investigating the hydrodynamic behavior of two phase flow in a trickle-bed. Liquid saturation and wetting efficiency are quantified from data with a spatial resolution of 86 μm^3. An example for the applied data analysis procedure is illustrated in Fig. 3. In order to determine the voidage of a slice, an image was taken under conditions of zero flow and when the packed bed had been flooded with water (Fig. 3a). The ratio of wetting voxels ("white" voxels), that contain liquid, to all voxels of the whole packed bed gives the porosity of the catalyst bed. This image is considered as reference for the calculation of liquid saturation.

For determining the wetting efficiency, Fig. 3b was used as reference image, which was obtained by further data analysis from Fig. 3a to identify all voxels containing liquid–solid interfaces, i.e. surface voxels. It shows the maximal wetting efficiency ($\gamma_0 = 1$), which means that the catalyst surface is completely wetted. Fig. 3c shows the same slice as Fig. 3a but it is taken under conditions of trickle flow with a superficial gas velocity $u_g = 11\,\mathrm{mm/s}$ and a superficial liquid velocity $u_l = 0.2\,\mathrm{mm/s}$. Fig. 3d was derived from Fig. 3c by counting only the surface voxels. The ratio

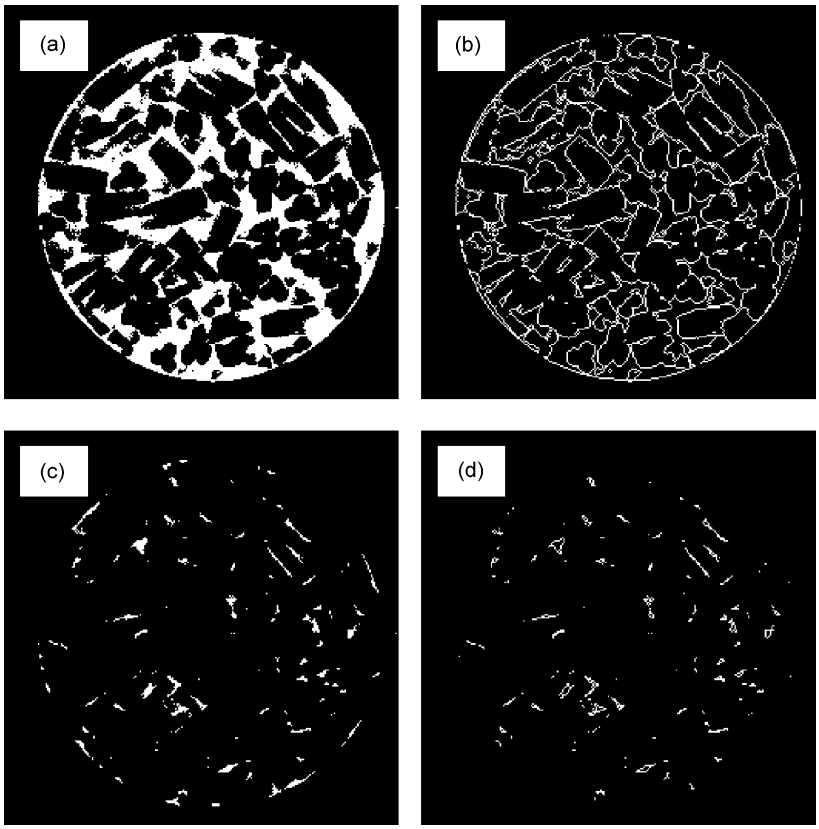

Fig. 3. Example of the data analysis procedure for NMR-imaging with water flow: (a) reference image for determining the void space acquired at zero flow of water; (b) the same slice as (a), only voxels containing liquid–solid contact surface voxels are identified; (c) image acquired under trickle flow condition for determining liquid saturation, $u_l = 0.21$ mm/s, $u_g = 11$ mm/s; (d) surface voxels at trickle flow.

of the number of wetting voxels in Fig. 3c to those in Fig. 3a is the liquid saturation at actual conditions of two-phase flow. Analogue, the ratio of the number of surface voxels in Fig. 3d to those in Fig. 3b gives the wetting efficiency.

Table 3 reports the liquid saturation and the wetting efficiency measured by MRI for a wider range of liquid flow rates than those used in the kinetic investigation with the trickle-bed reactor. It can be seen that liquid saturation and wetting efficiency both increase continuously with increasing liquid flow rates. At the lowest water velocity $u_l = 0.21$ mm/s, liquid saturation is 0.08 and reaches 0.3 at $u_l = 2.3$ mm/s. However, the results of this experiment with water and air would not compare to the results obtained by integral measurements of liquid saturation under real conditions (Table 2) with a laboratory trickle-bed reactor. Therefore, in the future MRI-experiments will be carried out with gas and diesel oil at high temperature and high pressure in order to validate the data from integral measurements.

Table 3
Liquid saturation and wetting efficiency from MRI measurements

u_g (mm/s)	11	11	11	11
u_l (mm/s)	0.21	0.44	1.5	2.3
β	0.08	0.16	0.21	0.30
γ	0.14	0.21	0.31	0.40

4.3. Modeling desulfurization

Considering LHSV as an important operating parameter the modeling of the desulfurization reactions and the reactor behavior in the lab scale seems to be

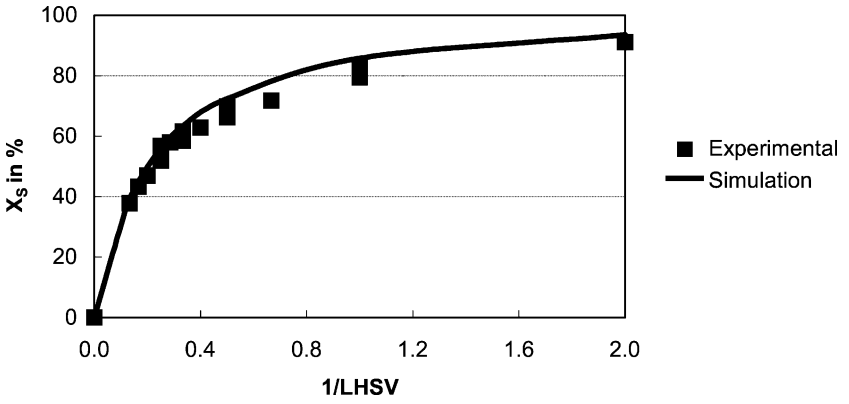

Fig. 4. Comparison of measured and calculated total sulfur conversion (Arabian Heavy, $T = 320\,^{\circ}\mathrm{C}$, $p = 40\,\mathrm{bar}$, $Q_g/Q_l = 200\,\mathrm{m^3/m^3}$, $y_{H_2S,0} = 1.4\%$).

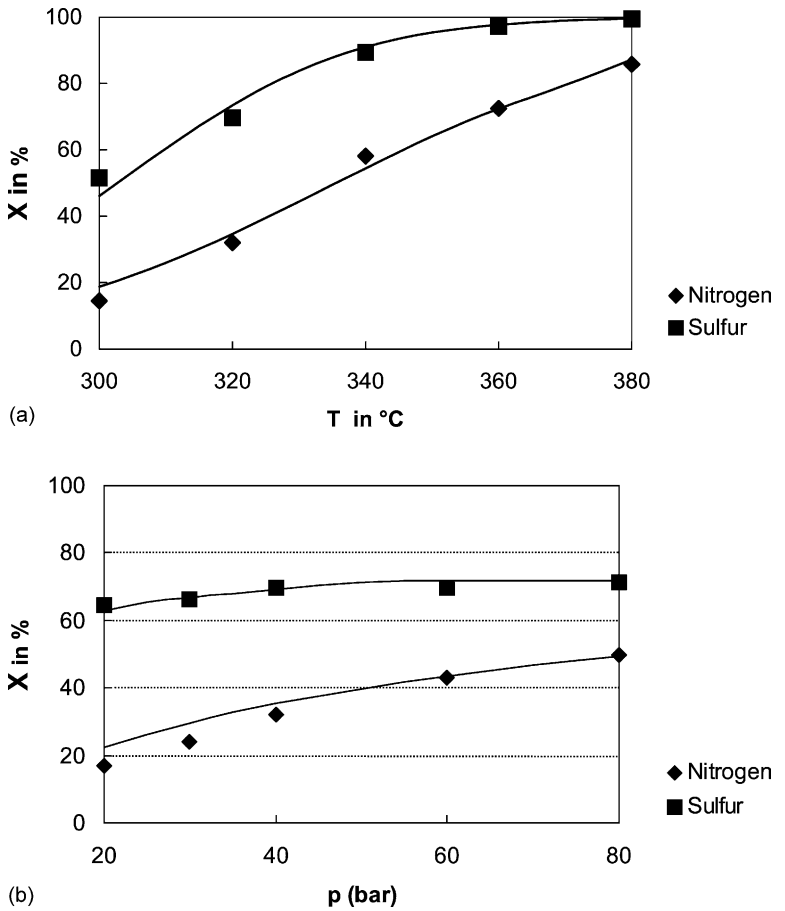

Fig. 5. Comparison of the experimental conversions of sulfur and nitrogen: (a) LHSV $= 2\,\mathrm{h^{-1}}$, $p = 40\,\mathrm{bar}$, $Q_g/Q_l = 200\,\mathrm{m^3/m^3}$, $y_{H_2S,0} = 1.4\%$ and (b) LHSV $= 2\,\mathrm{h^{-1}}$, $T = 320\,^{\circ}\mathrm{C}$, $Q_g/Q_l = 200\,\mathrm{m^3/m^3}$, $y_{H_2S,0} = 1.4\%$.

Table 4
Hydrocracking products from Arabian Heavy gasoil (LHSV = 2, $p = 40$ bar, $Q_g/Q_l = 200\,m^3/m^3$, $y_{H_2S,0} = 1.4\%$)

Concentration (wt.%)	Original	320 °C	340 °C	360 °C	380 °C
$C_{C_1-C_2}$	0	0.09	0.10	0.24	0.39
$C_{C_3-C_4}$	0	0.13	0.12	0.40	0.86
$C_{C_5-C_8}$	0	0.38	0.78	1.46	3.95

quite good (Fig. 4). Due to the simplification of the kinetics used for the sulfur reaction system and the wide distribution of reactivities, it is not surprising not to cover the total range of operation conditions.

Comparison of hydrotreatment results of the sulfurous and nitrogenous compounds show clearly the latter's low reactivity and the higher influence of hydrogen pressure on the nitrogenous (Fig. 5a and b). For hydrodenitrogenation the aromatic rings hydrogenation occurs before nitrogen removal. Hydrocracking results of the gas phase products are given in Table 4.

For the conversion of the sulfurous components hydrogen has to be spent. Using the model for prediction it should allow to calculate the specific hydrogen consumption $Q_{H_2/Oil}$. Taking the temperature as the operating parameter Fig. 6 shows that the initial hydrogen consumption (at 300–340 °C) is dominated by the reaction of the sulfurous and the aromatic compounds (the contribution of nitrogen is almost 0). The figures for $Q_{H_2/Oil}$ for the individual reactions have been calculated from hydrogen balances based on the measured conversions. The model predicts the "negative conversion" of aromatics above 350 °C. However, the hydrogen consumption does not decrease in the same quantity due to the starting of the hydrocracking reactions.

To perform a process evaluation various cuts from Arabian Heavy SGO were made and mixtures of them with LGO (total sulfur of 1700 ppm) which were individually desulfurized. The sulfur components in LGO (mainly benzothiophene) react completely and LGO can be considered like a diluent in the system. Diluent is used to avoid the generation of large quantities of distillation products needed to realize the experiments. The fractionation was done in a vacuum distillation (NORMAG) at 10 mbar with five theoretical plates and $L/d = 1$. The desulfurization results are summarized in Table 5 taking the finally achieved sulfur content as a criteria.

Obviously, dilution with a light fraction makes the hydrodesulfurization much easier (upper part of Table 5), and the bottom product of the distillation remains hard to be desulfurized.

4.4. Modeling the process

For the simulation the hydrotreating process is considered in its standard configuration [8]. The recycled stream of H_2/H_2S is not purified, only the recycle compression energy is calculated. The scale up factors

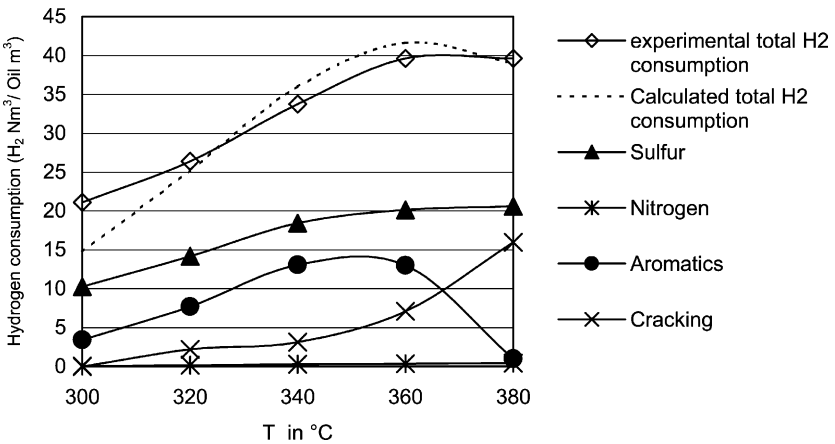

Fig. 6. Experimental total hydrogen consumption and contribution of each reaction on basis of experimental conversion and calculated hydrogen balance (Arabian Heavy, $p = 40$ bar, $Q_g/Q_l = 200\,m^3/m^3$, $y_{H_2S,0} = 1.4\%$).

Table 5
Outlet sulfur concentrations in ppm S of different fractions and mixtures of an Arabian Heavy gasoil ($p = 40$ bar, $Q_g/Q_l = 200\,m^3/m^3$, $y_{H_2S,0} = 1.4\%$)

Fraction	Original (ppm S)	T (°C), LHSV = 2 h^{-1}				
		300	320	340	360	380
90% LGO + 0–10% SGO	2570	<10	<10	<10	<10	<10
80% LGO + 0–20% SGO	3820	180	13	<10	<10	<10
65% LGO + 0–35% SGO	6060	765	115	<10	<10	<10
45% LGO + 0–55% SGO	9390	3630	1300	250	<10	<10
25% LGO + 0–75% SGO	12600	6600	3160	870	170	<10
10–100%	17460	9180	5780	2620	940	215
20–100%	17670	10040	6370	2570	710	330
35–100%	17920	11940	8000	3580	1080	405
55–100%	18140	10900	7130	3390	1060	410
75–100%	17730	10960	7490	3540	1200	345

Table 6
Data for the scale up from bench scale to industrial reactor size

	Bench scale	Industrial scale	Conditions
m_{cat}	0.030 kg	172.000 kg	LHSV = 2 h^{-1}
L	250 mm	30.000 mm	$T = 320$ °C
d_R	19 mm	3.000 mm	$p = 40$ bar
d_p	0.2 (1.5 mm)	1.5 mm	$Q_{gas}/Q_{oil} = 400\,m^3/m^3$
Re_l	0.08	11	$y_{H_2S,0} = 1.4\%$
Re_g	0.15	91	$\rho_l = 620\,kg/m^3$
F_{oil}	69 g/h	60 t/h	$\eta_l = 1.3 \times 10^{-4}$ N s/m^2
	Isotherm	Adiabatic	$\rho_g = 15\,kg/m^3$
			$\eta_g = 1.7 \times 10^{-5}$ N s/m^2

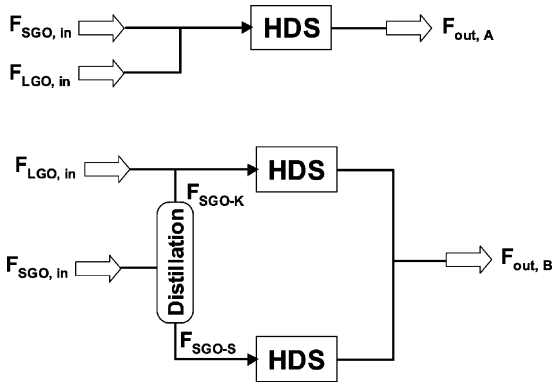

Fig. 7. Alternative process arrangements: (A) one reactor without fractionation and (B) two reactors in parallel with fractionated feeds.

from bench scale reactor to the industrial scale used are shown in Table 6. The major change between the two models is the adiabatic condition in the industrial reactor (see Section 3). Table 7 shows which type of information can be obtained by the simulation. The results will be discussed elsewhere [9].

Based on the results reported in Table 5 two alternative process configurations as per Fig. 7 are compared. An example of the evaluation of the two alternative processes in Fig. 8 shows that no clear benefit is achieved by the fractionation.

Running the two reactors at different temperatures and targeting for a product of 500 ppm S a minimal advantage of 5 °C of the total process is achieved. For

Table 7
Modeling results for the hydrotreating process (Arabian Heavy, $Q_L = 70\,m^3/h$, NiMo/γ-Al_2O_3, $Q_g/Q_l = 400\,m^3/m^3$)

Sulfur content of product (ppm S)	Reactor inlet temperature (°C)	Pressure (bar)	Hydrogen consumption (m^3 H_2/m^3 oil)	Heat + power consumption of the process (MW)
2000	320	41	36.6	8.8 + 2.0
500	343	41	48	10.4 + 2.0
350	349	41	50	10.8 + 2.0
50	364	41	57	11.9 + 2.2
50	357	61	61	10.1 + 2.8

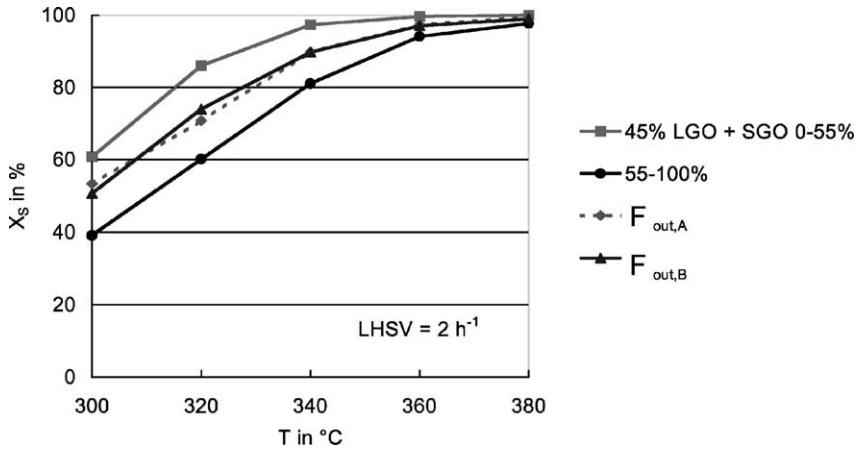

Fig. 8. Comparison of total sulfur conversion for processes (A) and (B) ($p = 40$ bar, $Q_g/Q_l = 200\,m^3/m^3$, $y_{H_2S,0} = 1.4\%$).

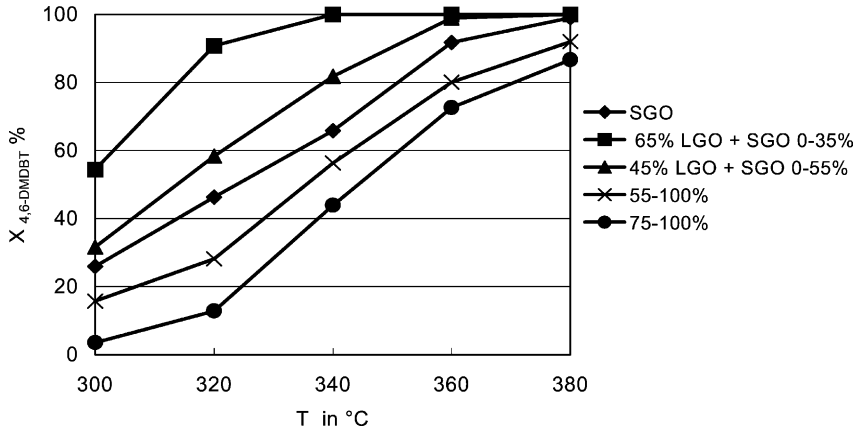

Fig. 9. Conversion of 4,6-DMDBT in different fractions of Arabian Heavy ($LHSV = 2\,h^{-1}$, $p = 40$ bar, $Q_g/Q_l = 200\,m^3/m^3$, $y_{H_2S,0} = 1.4\%$).

this calculation in process B, one reactor runs with a mixture of 45 wt.% LGO plus a fraction of SGO 0–55% at 340 °C and the second with the complementary 55–100% SGO fraction at 360 °C whereas the alternative process A runs at 355 °C.

Looking at the conversion X of one of the most refractive compounds, 4,6-DMDBT, in different cuts confirms the inhibition depending on the fraction or oil matrix (Fig. 9).

5. Conclusion

An extension of the modeling of the hydrotreating process to simulate hydrogen consumption was successfully realized. Simplified hydrocracking and hydrodenitrogenation reactions are added based on experimental results.

Inhibition by the oil matrix was confirmed in trickle-bed reactors. Only distillation for the generation of different cuts does not generate a synergistic effect to reduce the total matrix inhibition. The use of selective separation (elution) may offer an opportunity to extract inhibiting components.

MRI has proved to be a useful tool in visualization of liquid distribution in packed beds. The application of image analysis allows us to determine the liquid saturation and the wetting efficiency within the bed. The long term objective of this work is to develop an MRI-technique for measuring the distribution and the

velocity of gas and diesel oil in a trickle-bed under the conditions of high temperature and pressure. The results from MRI-investigations on hydrodynamics will be used to modify the existing model for hydrotreating of middle distillates.

References

[1] Commission of the European communities, Proposal for a directive of the European parliament and the council on the quality of petrol and diesel fuels and amending directive, 98/70/EC COM(2001) 241 final.
[2] H. Schulz, W. Böhringer, P. Waller, F. Ousmanov, Gas oil deep hydrodesulfurization: refractory compounds and retarded kinetics, Catal. Today 49 (1999) 87–97.
[3] H. Korsten, U. Hoffmann, Three-phase reactor model for hydrotreating in pilot trickle-bed reactors, AIChE J. 42 (5) (1996) 1350–1360.
[4] P.T. Callaghan, Principles of Nuclear Magnetic Resonance Microscopy, Clarendon Press, Oxford, 1991.
[5] A.J. Sedermann, L.F. Gladden, Magnetic resonance imaging as a quantitative probe of gas–liquid distribution and wetting efficiency in trickle-bed reactors, Chem. Eng. Sci. 56 (8) (2001) 162–2615.
[6] R. Chowdhury, E. Pedernera, R. Reimert, Trickle-bed reactor model for desulfurization and dearomatization of diesel, AIChE J. 48 (1) (2002) 126–135.
[7] W.J.A. Wammes, J. Middelkamp, W.J. Huisman, C.M. deBaas, K.R. Westerterp, Hydrodynamics in a cocurrent gas–liquid trickle bed at elevated pressures, AIChE J. 37 (1991) 1849–1862.
[8] C. Jentsch, Erdölverarbeitung, Ullmanns Encyklopädie der technischen Chemie, 4. Auflage, Band 10, Verlag Chemie, Weinheim, 1975, pp. 641–714.
[9] E. Pedernera, Dissertation, Universität Karlsruhe, 2003.
[10] S. Goto, J.M. Smith, Trickle-bed reactor performance. I. Holdup and mass transfer effects, AIChE J. 21 (4) (1975) 706–713.
[11] M.J. Girgis, B.C. Gates, Reactivities, reaction networks and kinetics in high-pressure catalytic hydrotreating, Ind. Eng. Chem. Res. 30 (9) (1991) 2021–2058.